Theor Chem Acc (2015) 134:4
DOI 10.1007/s00214-014-1606-2

REGULAR ARTICLE

Theoretical investigation on $SnCl_4$-catalyzed tandem dimerization/oxy-2-azonia-Cope rearrangements between β,γ-unsaturated ketones and imines

Liang Zhang · Jing-Mei Wang · Quan-Rui Wang · Dan-Wei Zhang · Zhan-Ting Li · Zhi-Ming Li

Received: 19 September 2014 / Accepted: 10 December 2014 / Published online: 11 January 2015

Abstract The mechanism of the Lewis acid-catalyzed oxy-2-azonia-Cope rearrangement between β,γ-unsaturated ketones and imines leading to the formation of homoallylic amides and lactams has been theoretically studied using the B3LYP density functional theory methods enhanced with a polarized continuum solvation model. It was predicted that the $SnCl_4$-catalyzed tandem dimerization/oxy-2-azonia-Cope rearrangement mechanism is highly preferred over the uncatalyzed version as well as the plausible tandem dimerization/Prins rearrangement mechanism. A two-step pathway was found for the overall reaction, involving the initial nucleophilic dimerization followed by the [3,3]-sigmatropic rearrangement. The latter phase was considered to be the rate-limiting step. Particularly, the transition states account for the experimentally observed stereoselectivities and *Z*/*E* selectivities. The high stereoselectivity and *Z*/*E* selectivity for the chiral cyclic substrates can be attributed to the relative conformational stabilities of TSs. Moreover, distortion–interaction analysis has been performed in an attempt to quantify the various contributions to the reaction transition states, and it revealed that interaction energy $E_{\text{int}}^{\text{II}}$ and distortion energy $\Delta E_{\text{d}}^{\text{I}}$ associated with the formation of the **2COM2** complex are the determining factors to define the *Z*/*E* selectivities for nine- and ten-membered ring pathway, respectively. Investigation on the ethyleneimine-involved reaction predicts a relatively very low barrier in the pathway; thus, the sequence might be a useful strategy for synthesis of macrolactams.

Keywords Oxy-2-azonia-Cope rearrangement · Prins rearrangement · Density functional theory · β,γ-Unsaturated ketone · Distortion–interaction analysis

1 Introduction

Stereoselective [3,3]-sigmatropic rearrangements have developed into a generally powerful tool for construction of carbon–carbon as well as carbon–heteroatom bonds in organic synthesis [1–3]. Among them, both of the Claisen [4–6] and Cope [7–9] rearrangements have aroused exceptionally great interests in the past decades. The rearrangement of N-substituted 1,5-dienes is known as the aza-Cope rearrangement. This reaction has many variants, namely 1-aza-, 2-aza-, 3-aza- and various diaza-Cope rearrangements [10]. One of the inherent major problems of the reaction is the reversibility of the process. For driving the 2-azonia-Cope rearrangements to completion, Overman's tandem 2-aza-Cope rearrangement (2-azonia-[3,3]-sigmatropic rearrangement) and Mannich reaction are remarkable, which have provided impressive methods for the rapid assembly of pyrrolidine-containing structures [11, 12]. As with all [3,3]-sigmatropic rearrangements, the activation energies can be significantly lowered when the starting 1,5-diene system is charged, and under these cases, the reaction takes place at a lower temperature.

Quite recently, we have uncovered a new variant for the 2-azonia-[3,3]-sigmatropic rearrangement [13, 14]. Thus,

Electronic supplementary material The online version of this article (doi:10.1007/s00214-014-1606-2) contains supplementary material, which is available to authorized users.

L. Zhang · Q.-R. Wang · D.-W. Zhang · Z.-T. Li · Z.-M. Li (✉)
Department of Chemistry, Fudan University, 220 Handan Road, Shanghai 200433, China
e-mail: zmli@fudan.edu.cn

J.-M. Wang
Research Centre for Analysis & Measurement, Fudan University, Shanghai 200433, China

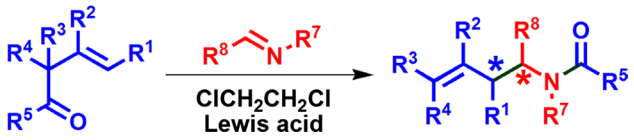

Scheme 1 Oxy-2-azonia-Cope rearrangement

in the presence of a Lewis acid, β,γ-unsaturated ketones and oximes undergo nucleophilic addition to produce dimeric zwitterionic intermediates, and subsequent 2-azonia-Cope rearrangements to afford homoallylic amides (Scheme 1). We have termed this new variant as oxy-2-azonia-Cope rearrangement. This strategy is featured by overcoming the reversibility problem with formation of an amide bond and has been utilized for the synthesis of functionalized allyl α-amino acid derivatives with imino ethyl glyoxalates as the substrates [14].

Although various 2-azonia-Cope rearrangements have found a myriad of applications in organic synthesis, the theoretical investigation is, however, anecdotal [13, 15]. An important theoretical approach to the mechanism has recently been devoted to these rearrangements by P. Merino and coworkers. They disclosed that the located transition states of 2-azonia-Cope rearrangements of cyclic nitrones have a chair-like conformation, and the uncatalyzed process proceeds through a neutral transition state, while the catalyzed process takes place through cationic species [15]. We have proposed in our recent work that, in the $EtAlCl_2$-catalyzed oxy-2-azonia-Cope rearrangement reaction, the chair-like transition states are generally preferred over boat-like ones, and the [3,3]-sigmatropic rearrangement step is the rate- and product-determining step despite of a high-energy preequilibrium in the formation of zwitterionic intermediates [13]. However, this initial hypothesis for the mechanism was put forward by the density functional theory (DFT) study on a single rearrangement reaction of a rigid cyclic β,γ-unsaturated carbonyl compound and an oxime ether [13].

In this paper, the mechanisms of this novel variant of 2-azonia-Cope rearrangement under catalysis of $SnCl_4$ have been investigated by theoretical calculations. The research was aimed at getting a general overview of the mechanism, especially the stereochemistry defining step of the reaction. The outcome would be informative for achieving a rationale of the substrate reactivity scope of the reaction. First, we interpreted that the Cope-type pathway is preferred with respect to the alternative Prins-type mechanism in the template reaction. Then, we probe deeply into the key influencing factors for the observed high chirality transfer using a ten-membered ring lactam case as the model. In addition, the discrepancy of *Z*/*E* selectivity in nine-membered ring and ten-membered ring lactam reaction (with reverse selectivity) was examined particularly by adopting transition state theory, nature bond orbital analysis and distortion/interaction analysis. Furthermore, the non-substituted ethyleneimine was utilized to explore the scope of this novel rearrangement reaction. The result indicates that it is a promising strategy for the synthesis of macrolactams via this $SnCl_4$-catalyzed tandem nucleophilic addition reaction. The localized orbital locator (LOL) and reduced density gradient (RDG) functions based on localized electron analysis were also used to analyze the covalent bond and non-covalent interactions in order to unravel the mechanism of the title reactions.

2 Computational method

All calculations were carried out using the B3LYP functional in Gaussian 09 program package [16]. Considering the previous work, the small-core, quasi-relativistic Stuttgart/Dresden effective core potential (standard SDD basis set in Gaussian 09) basis set was applied for Sn [17, 18]. The standard 6-31+G(d,p) basis set, which is pervasively used to investigate similar reactions, was used for C, H, O, N and Cl atoms [19–21]. Geometry optimizations of all minima and transition states involved were implemented at the chosen level of theory. To confirm that all of the stationery points are indeed the minima or first-order saddle points, frequency calculations were conducted at the same level. Free energy at 298.15 K was computed that included entropic contributions by considering the vibration, rotation and translational motions. The intrinsic reaction coordinate (IRC) pathway was traced to identify the transition state [22, 23]. Solvent effects were treated in single-point calculations on the gas-phase optimized structures, using the polarizable continuum solvation model (PCM) with dichloroethane as a solvent with UFF radii [24–28]. The natural population analysis (NPA) [29] allows the evaluation of the charge transfer degree and the direction between the reactants parts at the **TS**s. The charge transfer discussed in the context is in terms of the residual charge on the oxime ether (or imine fragment). In addition, second-order perturbation theory analysis of the Fock matrix can evaluate the donor–acceptor interaction in the NBO basis [30].

LOL [31] and RDG [32] functions have been used to study the covalent bond and non-covalent interactions for some stationary points in our studied reactions. LOL is based on the electron kinetic energy density as a measure of electron localization. It gives simple, recognizable patterns in classic chemical bonds and proves useful in interpreting the structure using graphical representations. And it is referenced with a LOL value of 0.5. Values of LOL larger than 0.5 are characteristic of regions with localized electrons, typical of covalent bonding and lone pairs, and these are shown as green, yellow and red in LOL maps. LOL values smaller than 0.5 are characterized by delocalized electrons and are typical of regions with multicenter bonding shown

in deep blue, blue and light blue in LOL contour plots. In order to investigate the weak interactions in real space based on the electron density and its derivatives, RDG was developed by Johnson et al. The RDG is a fundamental dimensionless quantity coming from the density and its first derivative. Its density tails show that large, negative values of sign(λ^2)ρ are indicative of attractive interactions (such as dipole–dipole or hydrogen bonding), while if sign(λ^2)ρ is large and positive, the interaction is non-bonding. Values near zero indicate very weak, van der Waals interactions. The sign of λ^2 is utilized to distinguish the bonded ($\lambda^2 < 0$) from non-bonded ($\lambda^2 > 0$) interactions [32]. Multiwfn package, version 2.1 [33], has been employed for LOL and RDG analysis using the wavefunction obtained from the same calculation level described above.

To identify the stable structures of the reactants including β,γ-unsaturated ketone and oxime ether, the relaxed scans were carried out at B3LYP/6-31+G(d,p) level in gas phase, and the scan results are presented in Figure S1-S4. Afterwards, the lowest local minima on the potential energy curves were optimized at the same level. The stable conformers and the absolute energies of the reactants are shown in Table S1.

3 Results and discussion

3.1 The mechanism of the template reaction (the Cope pathway vs. the Prins pathway)

First, we selected the $SnCl_4$-catalyzed tandem nucleophilic addition reaction of the acyclic carbonyl compound **1a** and the oxime ether **1b** as the template reaction to study the possible mechanism (see Scheme 2). The product **1P** can be formed through oxy-2-azonia-Cope rearrangement [13]. Nevertheless, it could be produced alternatively in a Prins-type [34, 35] manner by coordination of the Lewis acid $SnCl_4$ to the N atom of oxime **1b**, as illustrated in Scheme 2. In this work, the coordination manner of $SnCl_4$ to the oxime was assigned to form a chelate having a trigonal bipyramidal geometry [36].

The computational results are shown in Fig. 1, and the relevant stationary point structures are shown in Fig. 2. For clarity, only the lowest energy pathway for Cope and Prins reaction is presented in Fig. 1. In both energy profiles, only the chair-like transition states are involved, which is in agreement with a typical Cope and Prins rearrangement (see Electronic supplementary material). For **1Cope-TS** in the Cope pathway, the lowest energy chair-like geometry is 13.4 kcal/mol more stable than the lowest energy boat-like one, which is attributable to the strain due to the annulated ring system. The axial disposition of $SnCl_4$ in both pathways is favored over the pseudo-equational one, which is determined by the required orientation of the orbitals involved in the rearrangement [13, 15].

For the Cope pathway with the lowest energy, reactant **1a** is firstly activated by coordination of $SnCl_4$ to the carbonyl group to generate **1Cope-COM1**. Upon addition of oxime ether **1b**, the zwitterionic complex **1Cope-COM2** is formed via **1TSCOM12**. In **1Cope-COM2**, 0.516 e charge is transferred from oxime ether **1a** fragment to **1COM1** fragment. The distance between C4 and N29 turns to be only 1.60 Å, while the one between C6 and C22 is still 3.30 Å, far beyond bond forming (Fig. 2). Finally, $SnCl_4$

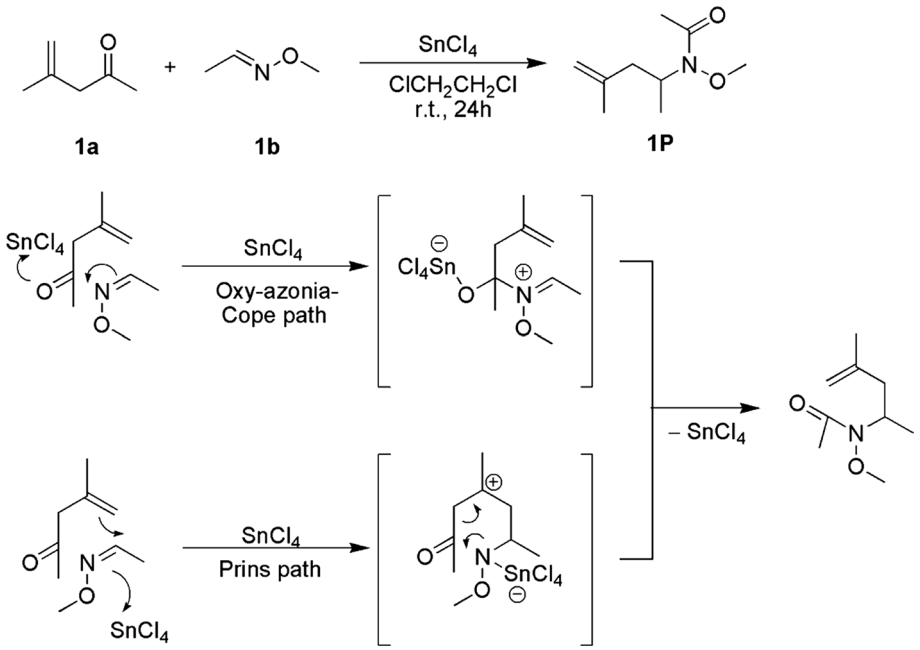

Scheme 2 Two plausible pathways for the reaction of **1a** and **1b**

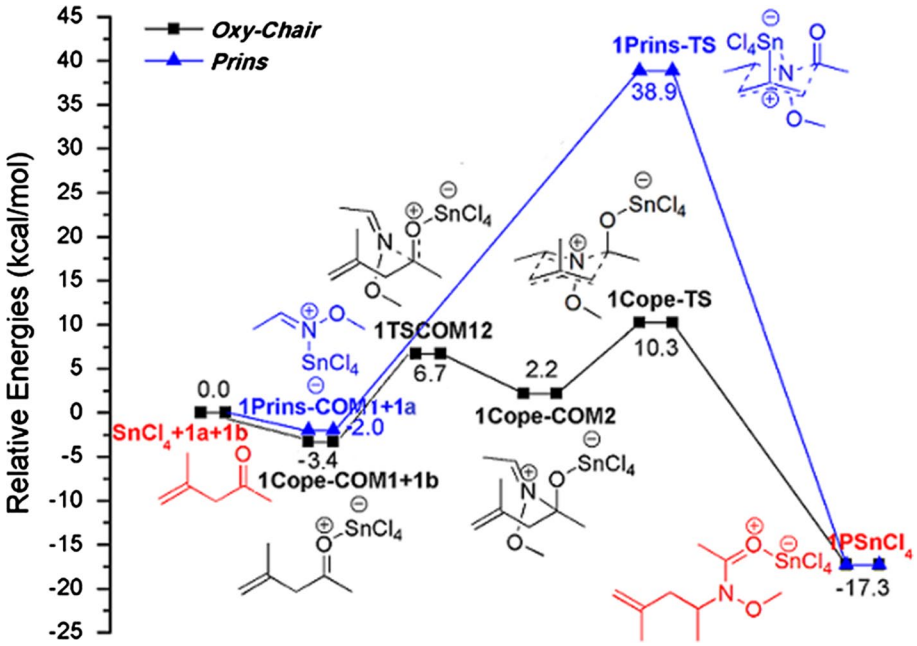

Fig. 1 Calculated [PCM (dichloroethane)/B3LYP/6-31+G(d,p)] free energy profiles for the rearrangement of **1a** and **1b**. Cope pathway is in black (*filled square line*), and the Prins one is in blue (*filled triangle line*)

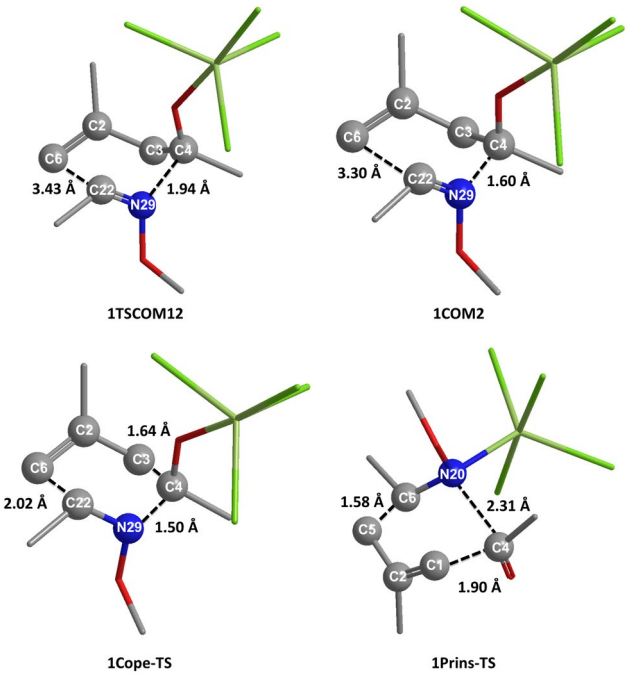

Fig. 2 Selected stationary points shown in Fig. 1

coordinated product **1PSnCl$_4$** is produced through Cope rearrangement transition state **1Cope-TS**. In **1TSCOM12** and **1Cope-TS**, C4–C3–C2–C6–C22–N29 formed a six-membered ring with chair-like conformation. From the NBO analysis of **1Cope-TS**, the bond orders of two newly formed σ bonds (C4–N29 and C6–C22) are 0.889 and 0.469, respectively. This inferred clearly that the Cope rearrangement step is a highly asynchronous concerted process [37–39]. It should be underlined that only the lowest chair-type process is two-step for the Cope pathways, which differs from other one-step processes including the boat-type paths of Cope and Prins paths (see Electronic supplementary material).

For lowest energy Prins pathway, the activation mode for the reactant **1a** is different. In this case, the Lewis acid is coordinated to the N atom of oxime ether **1b** instead of the O atom of the carbonyl group of **1a**. The forming **1Prins-COM1** is less stable than **1Cope-COM1** in Cope pathway by 7.7 kcal/mol. Without the generation of zwitterionic complex **1Prins-COM2**, the Prins rearrangement proceeds with a dramatically high barrier 40.9 kcal/mol to form the same product **1PSnCl$_4$**. These results are in good agreement with the recent theoretical study by Kraft et al. [40]. Comparison between the total barriers for the two paths shows a clear preference for Cope pathway whose total free energy barrier is only 10.3 kcal/mol, while that for the lowest Prins pathway 38.9 kcal/mol. The dramatically higher barrier for the Prins pathway may result from the electron-withdrawing inductive effect of the methoxy group. The effect prevents the perfect coordination of N atom with Sn compared to the free carbonyl oxygen atom in Cope pathway. The bond distance of N–Sn in **1Prins-TS** (2.24 Å) is 0.12 Å longer than that of O–Sn bond in **1Cope-TS** (2.12 Å), which proves the aforementioned effect of the methoxy group to some extent. This effect can be clearly expressed in color-filled contour-line diagrams of LOL isosurfaces (Fig. 3a, b). As shown in Fig. 3a, the interaction between O atom and Sn atom is very strong, and O–Sn bond is almost an ionic bond. The N–Sn bond is completely a covalent bond (Fig. 3b), however. In fact, $SnCl_4$ may not be a catalyst in the Prins pathway as

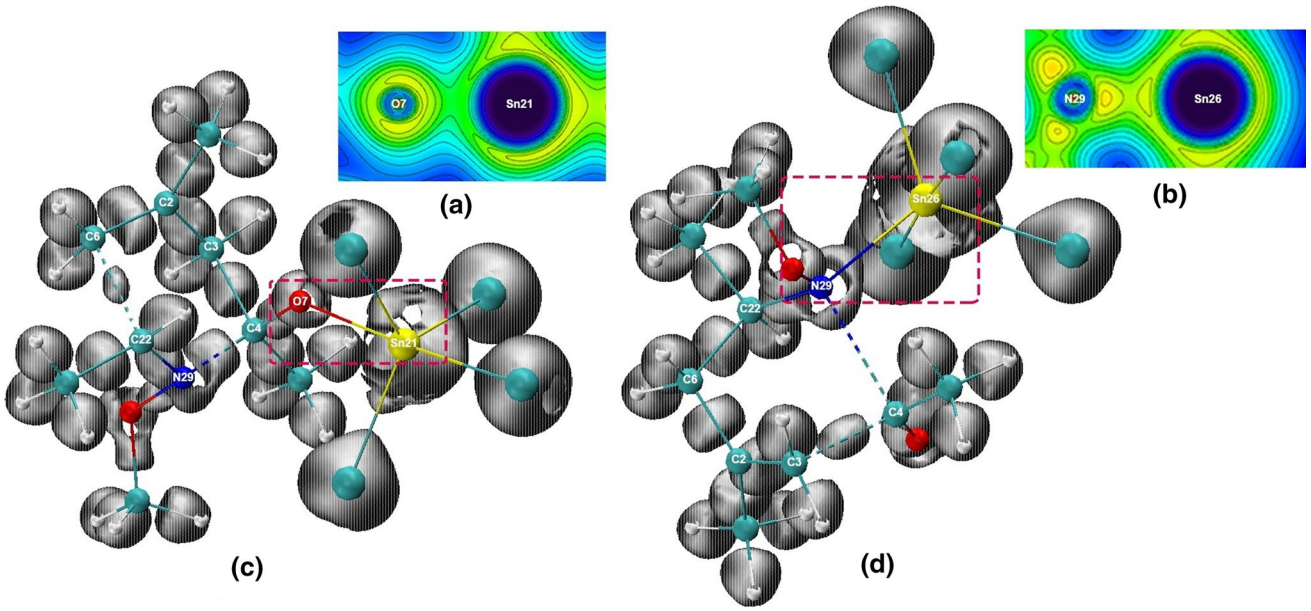

Fig. 3 *Color-filled contour-line* diagrams of LOL isosurfaces through the variable $v_\sigma = t_\sigma/(1 + t_\sigma)$ for part of **1Cope-TS** (**a**) and **1Prins-TS** (**b**); LOL isosurfaces ($v_\sigma = 1/2$ a.u.) for **1Cope-TS** (**c**) and **1Prins-TS** (**d**)

the barrier for non-catalyzed Prins pathway is 2.3 kcal/mol lower than that of the $SnCl_4$-catalyzed one in dichloroethane. No doubt binding $SnCl_4$ to N atom of the oxime ether **1b** increases the electrophilicity of C atom of double bond, while makes the N a weaker nucleophile and induces more steric hindrance, which leads to a higher overall barrier than the uncatalyzed Prins pathway.

The LOL analysis for **1Cope-TS** and **1Prins-TS** can also give valuable information for the preference of Cope pathway. As shown in Fig. 3c, in **1Cope-TS**, the bond regions of newly formed bonds C6–C22 and C4–N29 are circular cross sections and extend into the σ region. Particularly for C4–N29, the bond regions have more distinct shape and extend somewhat into the π region above and below the bond axis, which is considerably a little double-bond featured. As a result, these stronger interactions stabilize **1Cope-TS**. On the other hand, in **1Prins-TS** (Fig. 3d), there is nothing expressed above and below the bond axis of C4–N29 by the LOL analysis, which indicated that the covalent bond interaction of the atom N29 and C4 has not been formed yet, and the interaction between them is dominated by the weak electrostatic attraction. As for another newly formed bond (C6–C22), the bond regions around the bond axis corresponds to σ-region with a big and distinct circular cross section, where the typical single σ-bond is expected. Thus, two strong bonds forming interactions in **1Cope-TS** and just one strong bond forming interaction in **1Prins-TS** make Cope rearrangement as the preferred pathway. This is in good agreement with the conclusion from Fig. 1, the relative free energy of **1Cope-TS** is 28.6 kcal/mol dramatically lower than that of **1Prins-TS**.

In addition, it is worth noting that the Prins process is also asynchronously concerted. However, the C6–C22 is formed earlier than C4–N29 bond (Fig. 2). This is in reverse compared to the Cope path, in which C4–N29 bond forming is more advanced than bond C6–C22. That is to say, the C–N formation could be regarded vital for the Cope process, while in the Prins process it is the C–C bond forming. In **1Prins-TS**, C4–C3–C2–C6–C22–N29 also formed a six-membered ring with chair-like conformation.

To validate the above results from B3LYP/6-31+G(d,p) method, the two lowest pathways shown in Fig. 1 are recomputed at B2PLYP/6-31+G(d,p) level [41]. The results are shown in Fig. S5. The discrepancy between B3LYP and B2PLYP is on a range of 2.0–11.6 kcal/mol. Albeit the different relative values, the similar reaction profiles were obtained. And the same conclusion of Cope pathway's preference can be drawn. Thus, B3LYP/6-31+G(d,p) method is adopted throughout this work.

3.2 The mechanism investigation for formation of [$n + 4$] ring-expanded lactams

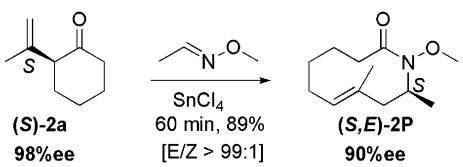

Encouraged by the initial results, we employed 2-vinylcycloalkanone (*S*)-**2a** to define the mechanism of the rigid substitutes, especially on the diastereoselectivity and *Z*/*E*

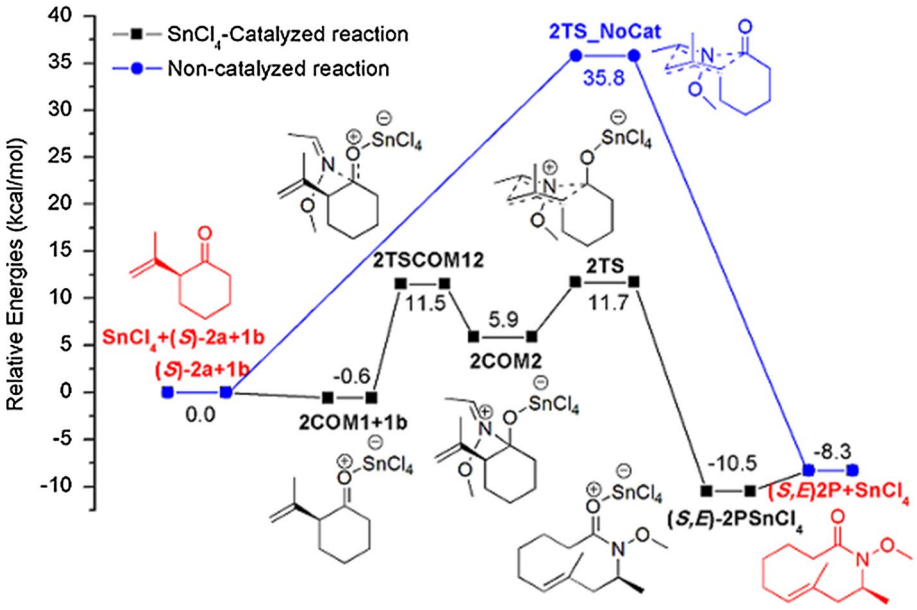

Fig. 4 Calculated [PCM(dichloroethane)/B3LYP/6-31+G(d,p)] free energy profiles for the $SnCl_4$-catalyzed reaction (in *black*) and the non-catalyzed reaction (in *blue*) pathway of **2a** and **1b** at the B3LYP/6-31+G(d,p) level

selectivity. According to our calculation results for the above reaction, with the solvent effect of dichloroethane taken into consideration (Fig. 4), the catalyzed reaction also features a two-step pathway in line with the former result: first generation of zwitterionic complex **2COM2** followed by the Cope rearrangement. The charge transfer from oxime ether moiety to ketone part in **2TS** is 0.243 e. The forming of C–O and C–C bonds is also asynchronous, and the degree of asynchronicity, in the Wiberg bond indexes, is 0.337 [42].

The results demonstrated that the non-catalyzed reaction was a one-step process without the formation of zwitterionic complex. And **2TS_NoCat** is similarly asynchronous with the catalyzed **2TS**. In addition, the charge transfer from oxime ether fragment to ketone fragment in **2TS-NoCat** is only 0.178 e (0.243 e in the catalyzed version). The corresponding transition states are shown in Fig. 5. The distance between C6 atom (C=O) and N12 atom decreased from 1.58 Å in **2TS_NoCat** to 1.49 Å in **2TS**, and the separation between C9 atom (C=C) and C11 atom (C=N) reduced distinctly from 2.22 Å in **2TS_NoCat** to 2.03 Å in **2TS**. These results must be accredited to the fact that the coordination of $SnCl_4$ prominently enhances the electrophilicity of C=O group, facilitates the charge transfer, thus dramatically reduces the reaction barrier from 35.8 to 11.7 kcal/mol and results in mild conditions for the tandem nucleophilic reactions.

Experimentally, the reaction of **2a** achieves not only a good yield but also a high diastereoselectivity. The possible stereochemistry processes of **2a** are presented in Scheme 3. The four chair-like and four boat-like processes were calculated. However, for clarity, only chair-like pathways are presented (Fig. 6). As inferred from Fig. 6, the profiles predict the *S,E* pathway as the most favored process, which is +2.9,

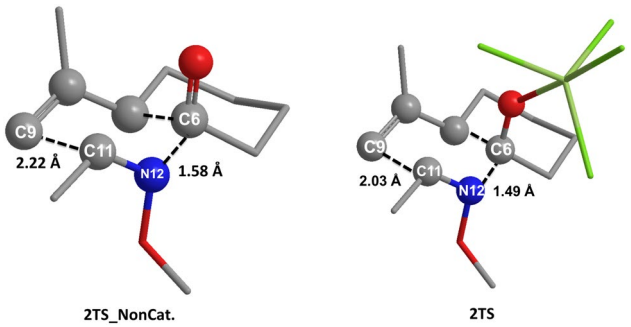

Fig. 5 Lowest TS conformations of rate-determining steps in the non-(*left*) and $SnCl_4$-catalyzed pathways of **2a** and **1b** (*right*)

+4.4 and +7.1 kcal/mol decrease of the total free energy barrier as compared to the other three processes, *RZ*, *RE* and *SZ*, respectively. The energy gaps between TSs were magnified in comparison with those of **2TSCOM12**s. For example, the gap between **2TSCOM12**s for *S,E* and *R,Z* is 0.8 kcal/mol, while the value is 2.9 kcal/mol between the corresponding **TS**s. This predicts briefly that the high diastereoselectivity is determined from the step of Cope rearrangement to a large extent. On the other hand, the stability orders of the stationary points at the same stages for different pathways are not identical. For instance, the order at **2TSCOM12** stage is *SE* > *RZ* > *SZ* > *RE*, while at **2TS** stage it turns to be *SE* > *RZ* > *RE* > *SZ*. This means that the selectivity trend of the four routes could not be maintained in the whole progress. But fortunately the *SE* pathway is always the most favorable, thus ensuring the high chirality transfer.

In order to understand the discrepancies in the route selection, we located eight feasible conformations of **2TSCOM12** and **2TS**, respectively, including four boat-like

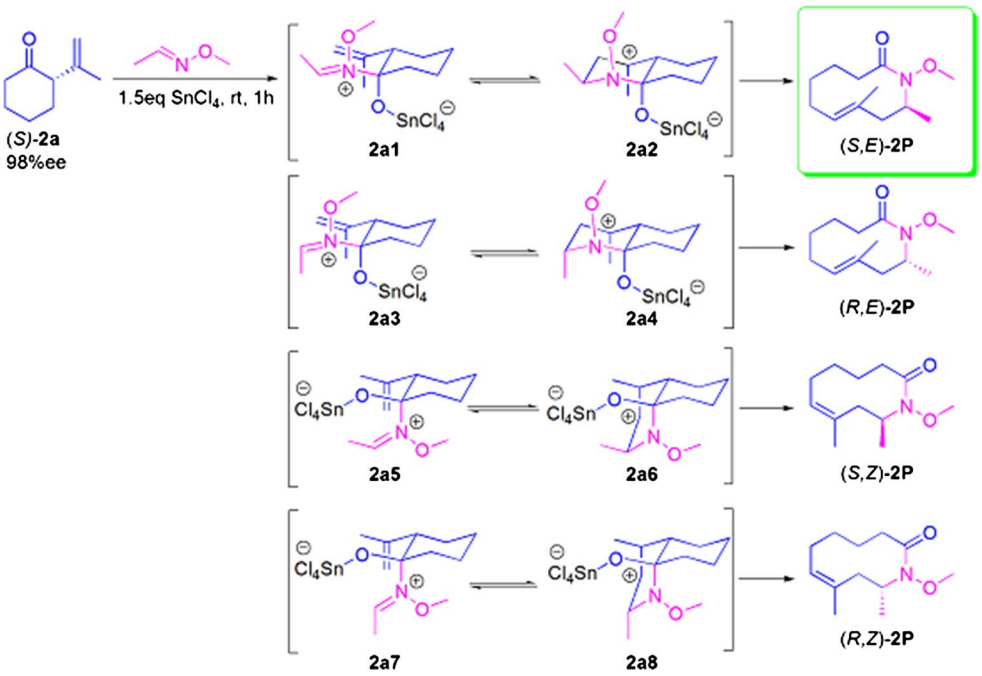

Scheme 3 Conceivable mechanism of *Z*/*E* selectivity for reaction of **2a** and **1b**

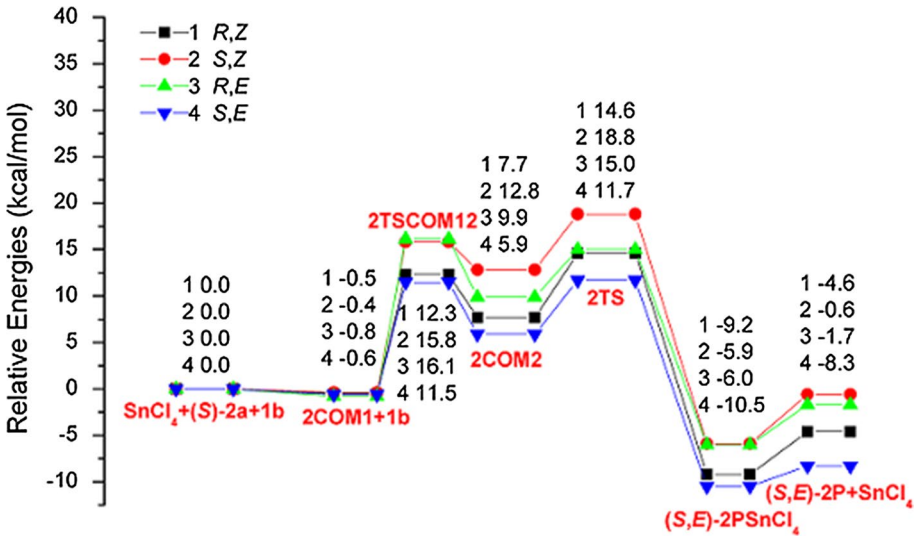

Fig. 6 Calculated [PCM(dichloroethane)/B3LYP/6-31+G(d,p)] free energy profiles for the chirality transfer pathway of **2a** and **1b**

and four chair-like geometries, which were provided in Fig. 7. The instability of other **2TSCOM12**s and **2TS**s compared to Chair-*S*,*E* version is obvious, and the most unstable structure is Boat-*S*,*E* version of **2TSCOM12** and **2TS**. The instabilities may be ascribed to three factors. The first is conformation of the backbone. For the Chair-*R*,*Z* **2TSCOM12** and **2TS**, as the second-lowest conformations, although the backbones are composed of two chair conformations, they are joined through an axial–equatorial union bond type. This conformation is less stable than the Chair-*S*,*E* version **2TS**s, because of relatively unfavorable nonbonded interactions within the concave area. In addition, the presence of the concave area also depresses the possibility for nucleophilic attack. Similar phenomena can also be found in Chair-*S*,*Z*, Boat-*R*,*E* and Boat-*S*,*E* cases. Second, the decrease of stability may also result from the twisted skeleton from a six-membered chair-like conformation to a six-membered boat-like one. The third possible influencing factor is the steric hindrance caused by the 1,3-diaxial repulsions between two methyl groups in C=C bond and C=N bond (labeled with red circles in Fig. 7), also presented in Chair-*R*,*E*, Chair-*S*,*Z*, Boat-*R*,*Z* and Boat-*S*,*E* cases. Under the synergistic effect of the three factors discussed above, the calculation results reveal that the Chair-*S*,*E* path is the most favored one and the Boat-*S*,*E* path displayed the highest energy transition structure of all counterparts.

The mechanism of this system may vary with the substitution pattern, and other transition states with slightly

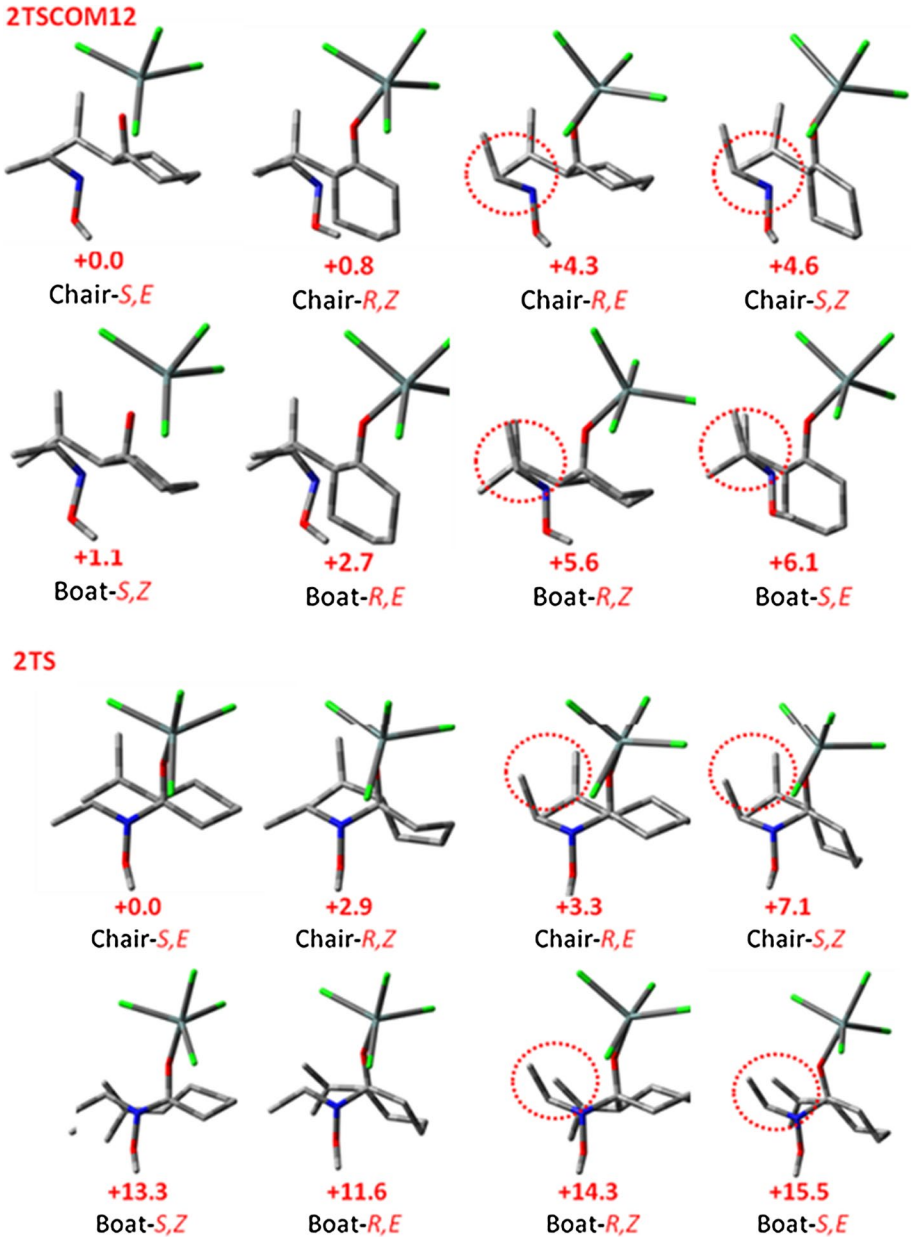

Fig. 7 Transition states for reaction of **2a**. Free energy ($\Delta\Delta G^{\ddagger}$) are given in kcal/mol. The hydrogen atoms are omitted, and the steric hindrances caused by the repulsive interaction between two methyl groups are labeled by *red circles*

different conformations may also come into play. However, the high diastereoselectivity observed in the reaction of **2a** and **1b** is well supported by our calculations since a pericyclic process with complete transfer of chirality is predicted for the rearrangement.

3.3 *Z*/*E* selectivity for nine-membered ring

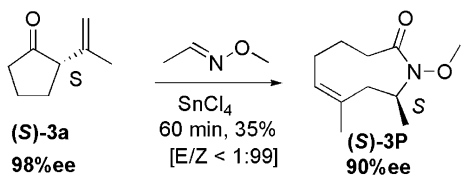

To get more details of the reaction mechanism for ring-shaped reactants, we next employed the five-membered (*S*)-**3a** as another substrate that also keeps intact in high chirality transfer, but has reversed *Z*/*E* selectivity to **2a**. The prior results for the reaction with **2a** revealed that only chair- like transition states should be taken into account in the pathway (Fig. 8). From the following potential energy surface in the solvent dichloroethane, we can see that the total barrier for *E* and *Z* pathway are 15.0 and 14.3 kcal/mol, respectively, and the *Z* product is thermodynamically 5.2 kcal/mol more stable than the *E* product. Thus, in line with the experimental findings, the *Z*-configuration product is favored both kinetically and thermodynamically. A

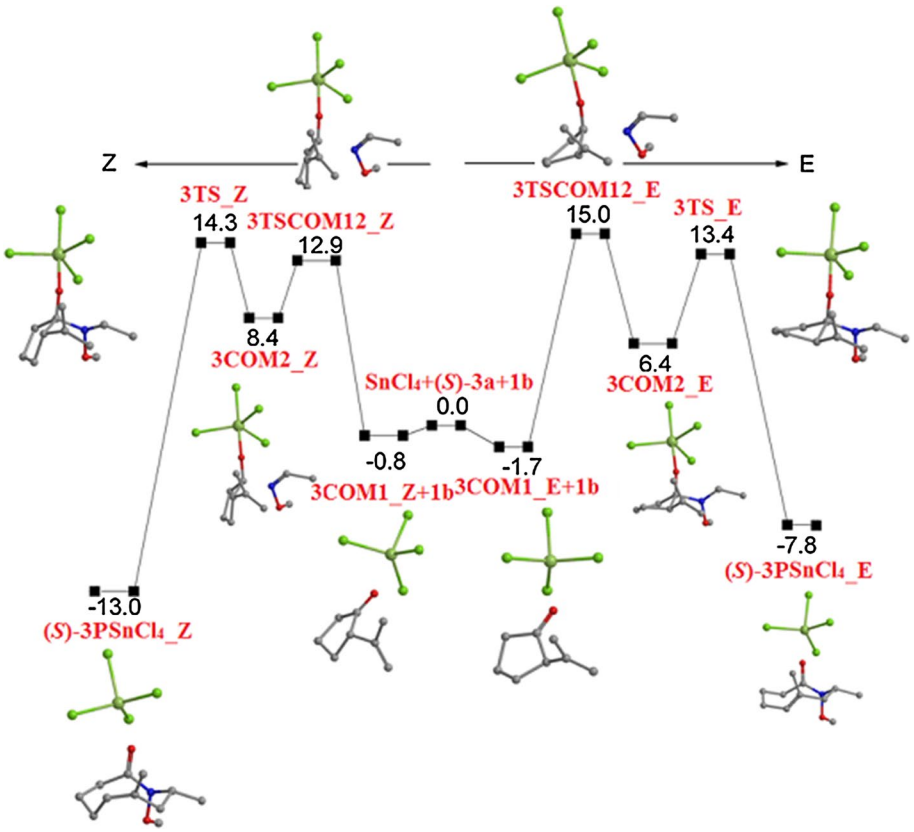

Fig. 8 Calculated [PCM(dichloroethane)/B3LYP/6-31+G(d,p)] free energy profiles for reaction of **3a** and **1b** (unit: kcal/mol)

small but significant difference between *Z* and *E* route is observed. For *E* pathway, the **3TSCOM12_E** presents the highest barrier, which suggests that the first phase is the rate-limiting step in the two-step process. But the situation is different in the *Z* pathway. At the meantime, the relative energy of **3TS_Z** is 0.9 kcal/mol higher than that of **3TS_E**, but 0.7 kcal/mol lower than that of **3TSCOM12_E** geometry, which results in a *Z*-selectivity in a balance of two aspects. The four conformations of the transition states are exhibited in Fig. 9, which elaborated the essential reasons for this case.

The charge transfer in terms of the residual charge on the imine fragment, for **3TSCOM12_E** and **3TSCOM12_Z**, is 0.289 and 0.355 e, respectively. This means that the direction of charge transfer is from imine moiety to **3a**, and the magnitudes reveal a more charge transfer for *Z* pathway, which may be the cause for the lower barrier of the first step for *Z* pathway [43]. According to the second-order perturbation theory analysis of the Fock matrix in NBO basis, there is more interaction between oxime ether part and $SnCl_4$ in **3TSCOM12_Z** (3.05 kcal/mol) than in **3TSCOM12_E** (2.46 kcal/mol). Also the distance between N atom of C=N and O atom of C=O in **3TSCOM12_E** is about 0.12 Å longer relative to

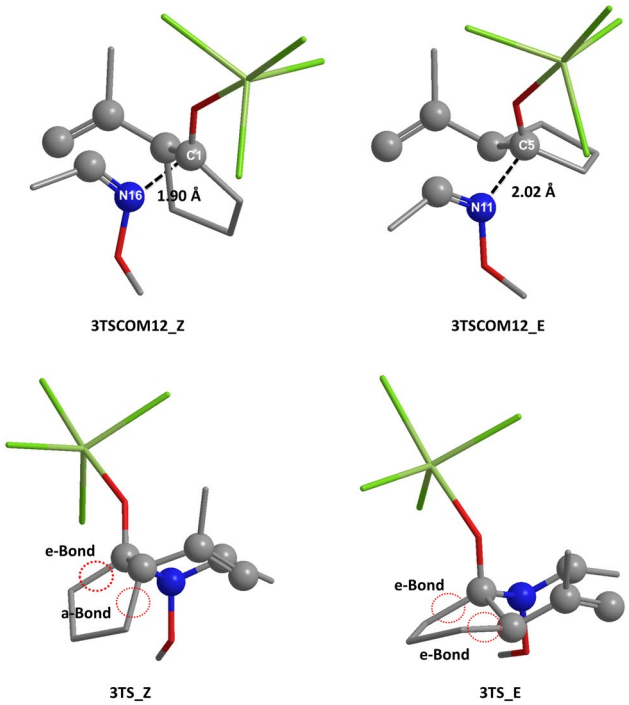

Fig. 9 Transition states for reaction of **3a** and **1b**

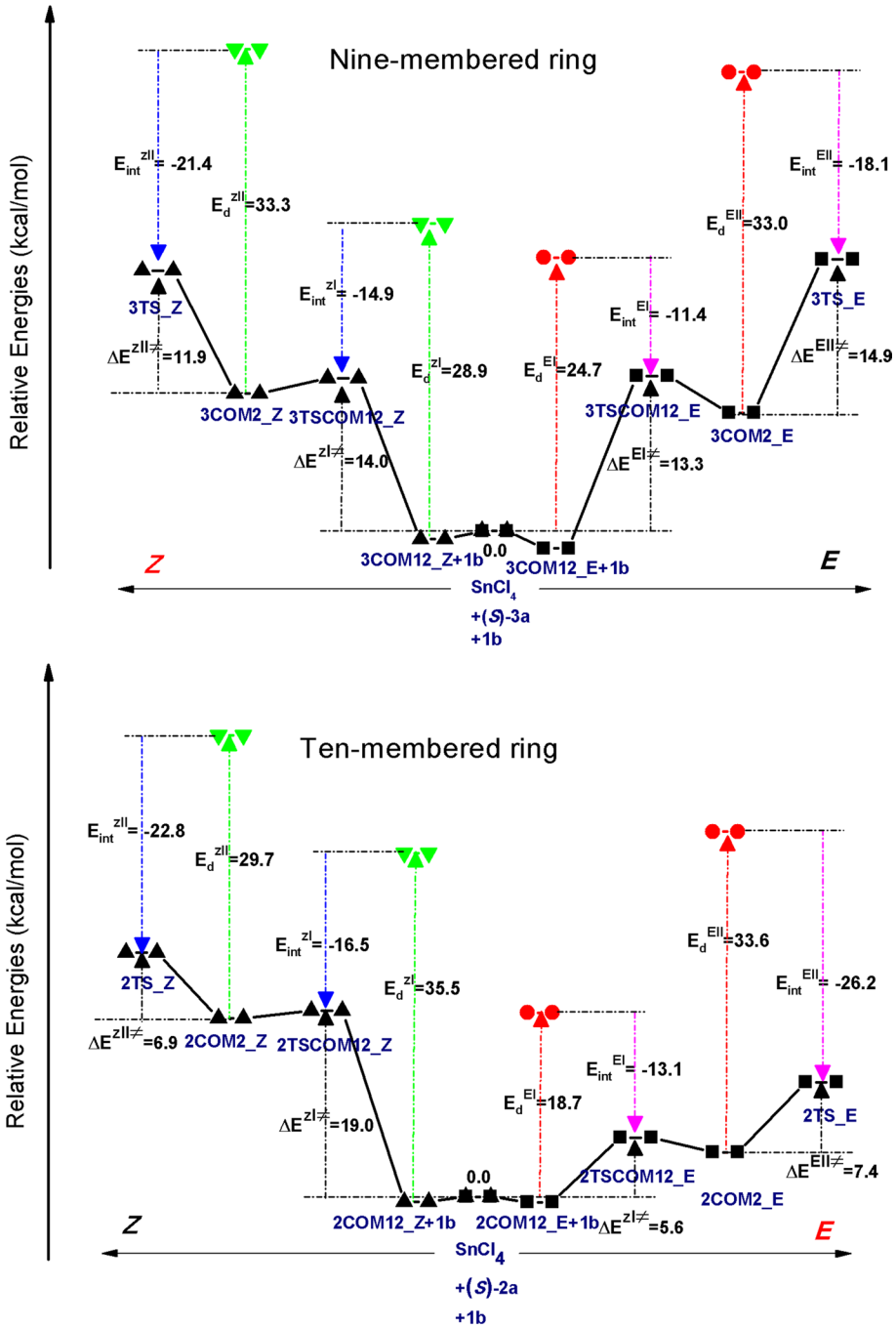

Scheme 4 Reaction pathway for nine- and ten-membered ring and distortion/interaction analysis

that in **3TSCOM12-Z** (see Fig. 9). Accompanied with the increase in the distance, a fairly weak charge transfer and less weak donor–acceptor interaction between reactant parts, a 15.0 kcal/mol barrier emerged for **3TSCOM12** in *E* pathway. However, the free energy of **3TS_E** decreases to 13.4 kcal/mol, less than that of **3TS_Z**, which should owe to the equatorial–equatorial bond union in the chair-like transition state structure (labeled by red circles in Fig. 9).

3.4 Distortion–interaction analysis for *Z*/*E* selectivity of nine- and ten-membered ring

To get a better understanding of *Z*/*E* selectivity for the [*n* + 4] ring-expanded lactams, a distortion–interaction analysis was performed for **TSCOM12**s and **TS**s in the pathway of nine- and ten-membered ring product [44–47]. The substrates are (*S*)-**3a** and (*S*)-**2a**, respectively. And only the lowest energy paths were considered.

Table 1 Electronic energies of **TSCOM12**s and **TS**s for the lowest energy pathway, $SnCl_4$-coordinated **2a**, **3a** and oxime ether **1b** distortion energies and sum of them, difference between distortion energies for **TS**s and **COM2**s, and interaction energies between $SnCl_4$-coordinated substrates and oxime ether **1b** (kcal/mol)

Path	ΔE^{I}	$E_d^I(SnCl_4\text{-Sub})$	$E_d^I(\mathbf{1b})$	E_d^I	E_{int}^I	ΔE^{II}	$E_d^{II}(SnCl_4\text{-Sub})$	$E_d^{II}(\mathbf{1b})$	E_d^{II}	E_{int}^{II}
9*E*	13.3	16.3	8.4	24.7	−11.4	14.9	21.8	11.2	33.0	−18.1
9*Z*	14.0	19.2	9.7	28.9	−14.9	11.9	21.2	12.1	33.3	−21.4
10*E*	5.6	9.8	8.9	18.7	−13.1	7.4	21.3	12.3	33.6	−26.2
10*Z*	19.0	25.5	10.0	35.5	−16.5	6.9	18.3	11.4	29.7	−22.8

This analysis allows quantification of individual contributions to the reaction barriers, from the distortion of the $SnCl_4$ complexes and oxime ether fragments, and interactions between them (Scheme 4; Table 1). As the analysis is performed generally in gas phase, and the reaction path is similar with that in solution, solvent correction is not employed for the pathway shown in Scheme 4. The distortion–interaction analysis revealed several factors that influence the *Z*/*E* selectivity. Firstly, for nine-membered ring pathways, interaction energy, E_{int}^{II}, is the determining factor that defines the *Z*/*E* selectivity, on account of that ΔE^{I} and ΔE_d^{II} are within 1 kcal/mol for the *Z* and *E* pathways, while E_{int}^{II} (−21.4 kcal/mol for *Z* vs. −18.1 kcal/mol for *E* process) almost exactly accounts for the 3 kcal/mol difference in ΔE^{II}. Secondly, for ten-membered ring pathways, unlike the nine-membered version, the two ΔE^{II} values are within only 1 kcal/mol, so E_{int}^{II} is not the factor controlling the *Z*/*E* selectivity. However, there is a 13.4 kcal/mol preference of ΔE^{I} for the *E* pathway. And the lower distortion energy associated with the formation of the **2COM2** complex in the *E* pathway mostly accounts for the energy difference, so ΔE_d^{I} is the factor that determines the *Z*/*E* selectivity. Thirdly, the only factor favoring **COM2**s and **PSnCl$_4$s** is the electronic interaction between the $SnCl_4$ complexes and the oxime ethers **1b**. Fourthly, in all the pathways, the major energy cost mainly comes from the distortion of the $SnCl_4$ complexes (E_d(**SnCl$_4$-Sub**)) as well as the distortion of oxime ethers (E_d(**1b**)). Fifthly, the geometries of oxime ethers are less perturbed in the structures of **TSCOM12**s and **TS**s, as can be seen from the lower values of the oxime ether distortion energies than those of the $SnCl_4$ complex.

3.5 Non-substituted imine substrate

In order to broaden the scope of this novel Cope rearrangement with regard to the tolerance of non-substituted imine substrate, the reaction between acetaldehyde imine (**2b**) and (*S*)-**2a** was employed for investigation. Note that only the *S,E* pathway is considered for clarity. The calculation result is shown in Fig. 10. The total pathway is two-step as well, involving the initial nucleophilic dimerization followed by the [3,3]-sigmatropic rearrangement. In **4TSCOM12**, the second-order perturbation theory analysis indicates a stronger interaction (4.56 kcal/mol) between imine fragment and $SnCl_4$ than those in **TSCOM12s** of nine- and ten-membered ring (e.g., 3.05 kcal/mol for **3TSCOM12-E** and 2.46 kcal/mol for **3TSCOM12-E**). The charge transfer in **4TS** is 0.268 e, also larger than that in oxime ether reactions. Such results should come from the absence of methoxy group, a group of electron-withdrawing inductive effect in character. In addition, this makes the charge on N atom of imine in **4TS** (−0.589 e) increase as well in comparison with the counterparts in oxime ether reactions (about −0.14 e). The inexistence of the methoxy group also shortens the distance between N atom (C=N) and C atom (C=O) in **4TS** to only 1.45 Å, about 0.05 Å shorter than the corresponding distance in **TS** of oxime ether reactions shown in Figs. 2 and 5.

The RDG analysis for **2TS** and **4TS** also indicates that the steric effect of the methoxy group will affect the stabilities of the two transition states (Fig. 11). In **2TS**, there are two areas of big lower density surface, which are corresponding to the repulsion interactions. One is between the methoxyl and the methyl group, the other is between methoxyl and the methylene group. However, in **4TS**, the express of the first big lower density surface between methoxyl and the methyl group disappeared and the area between methylene group and amino group decreases sharply, where the weak repulsion is expected. This indicated the repulsion in **2TS** is more strongly than that in **4TS**, which may be another cause for the higher stability of **4TS** than **2TS**.

Moreover, the variations between the gas phase and the solution phase are very obvious. The solvent dichloroethane can stabilize **4TSCOM12** and **4TS** sharply, but more for **4TS**; thus, the rate-determining step in solution is changed to **4TSCOM12** from **4TS** in gas phase. The total barrier in solution is only 2.1 kcal/mol, which can be easily surmounted under mild reaction conditions. It deserves comment since a new and efficient way to construct ring-expanded lactams could be excavated.

4 Conclusions

To sum up, our theoretical approach properly describes the Sn-catalyzed tandem nucleophilic addition of

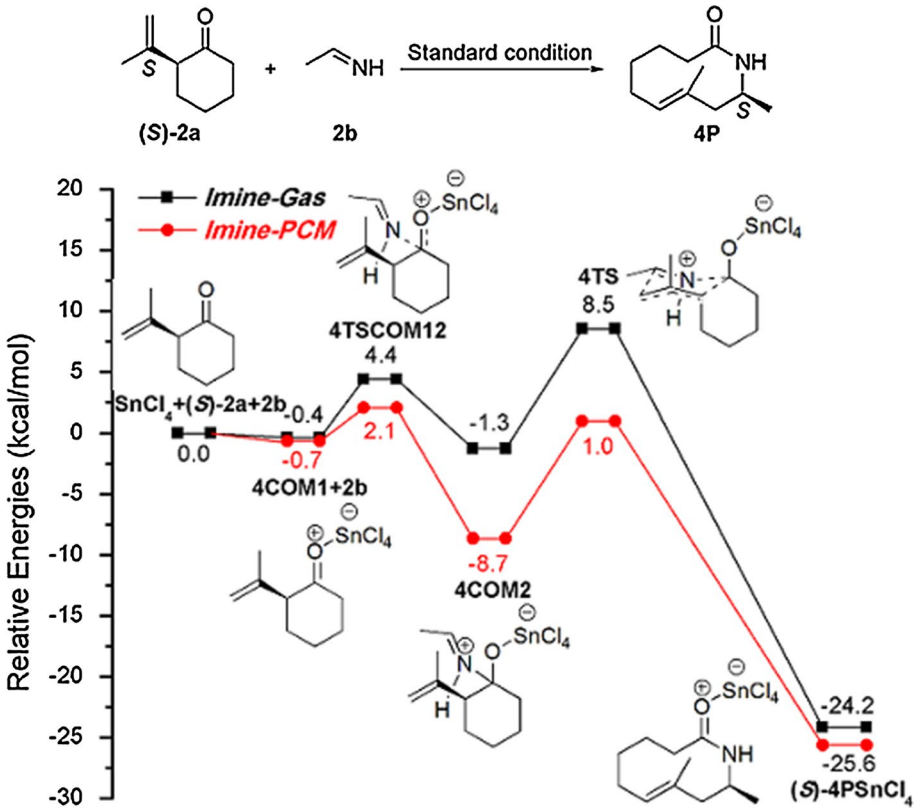

Fig. 10 Relative free energy profile in gas phase (*black line*) and in dichloroethane (*red line*) for the reaction of **2a** and ethanimine **2b** at the B3LYP/6-31+G(d,p) level

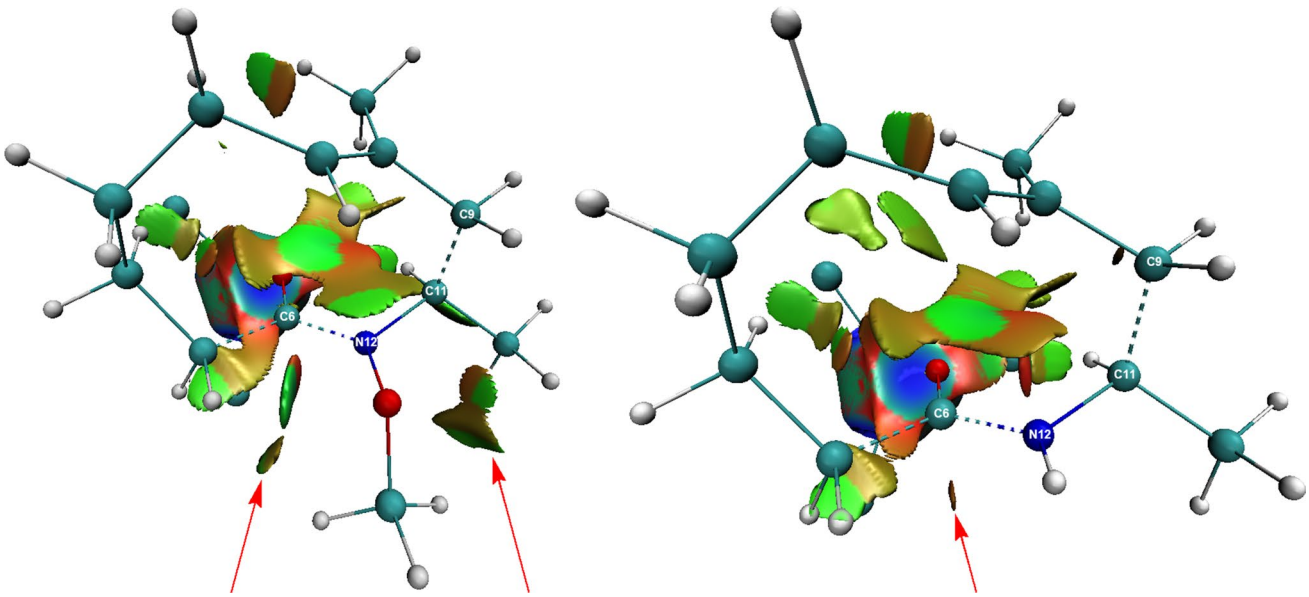

Fig. 11 Optimized geometries (B3LYP/6-31+G(d,p)) and gradient isosurfaces ($s = 1/2$ a.u.) for **2TS** (*left*) and **4TS** (*right*). The surfaces are colored on a *blue–green–red* scale according to the values of sign(λ^2)ρ, ranging from −0.04 to 0.02 a.u. *Blue* indicates strong attractive interactions, and *red* indicates strong non-bonded overlap

β,γ-unsaturated ketones with imines and the consecutive [3,3]-sigmatropic rearrangements leading to homoallylic amides. The calculated results provided an insight into the reaction mechanism and diastereoselectivity from microcosmic direction. DFT predicts that the $SnCl_4$-catalyzed tandem dimerization/oxy-2-azonia-Cope rearrangement

pathway between β,γ-unsaturated ketones and imines is highly preferred over non-catalyzed case as well as the tandem dimerization/Prins rearrangement pathway. Accordingly, a stepwise dimerization/oxy-2-azonia-Cope rearrangement mechanism was inferred for the reaction. The reaction is initiated by formation of zwitterionic intermediates that undergo consecutive Cope-type rearrangement as the rate-limiting step. Chair-like six-membered ring geometry of intermediates and TSs in Cope pathway always plays a predominant function in both flexible and rigid substrates. The solvent dichloroethane can effectually stabilize all transition states; thus, the barriers are decreased in the solution. Chirality-retention products can be obtained in ring-expanded lactam reactions from 2-vinylcycloalkanones. However, the *Z*/*E* selectivity may be altered with respect to the size of the ring. Our calculation results agree well with the experimental results. The high *Z*/*E* selectivity and chirality transfer are mainly governed by the conformational stabilities of TSs, including chair conformation over boat-like conformation, *e,e*-bond-type union over *a,e*-type one between two rings and 1,3-diaxial repulsion. Moreover, distortion–interaction analysis has been performed in an attempt to quantify the various contributions to the reaction transition states, and it revealed that interaction energy $E_{\text{int}}^{\text{II}}$ and distortion energy $\Delta E_{\text{d}}^{\text{I}}$ associated with the formation of the **2COM2** complex are the determining factors to define the *Z*/*E* selectivities for nine- and ten-membered ring pathways, respectively. The ethyleneimine-involved reaction reveals an extraordinary low barrier in the reaction path, thus envisioning a feasible route to lactams.

Acknowledgments Financial support from the National Natural Science Foundation of China (Nos. 21102019 and 21372045) is gratefully acknowledged.

Conflict of interest The authors declare that they have no conflict of interest.

References

1. Zeh J, Hiersemann M (2011) Stereoselective Synthesis 3. Stereoselective pericyclic reactions, cross-coupling and C–H and C–X activation. Thieme, New York
2. Ilardi EA, Stivala CE, Zkarian A (2009) Chem Soc Rev 38:3133–3148
3. Nubbemeyer U (2003) Synthesis, pp 961–1008
4. Hierseman M, Nubbemeyer U (2007) The Claisen rearrangement: methods and applications. Wiley-VCH, Germany
5. Ito H, Taguchi T (1999) Chem Soc Rev 28:43–50
6. Castro AMM (2004) Chem Rev 104:2939–3002
7. Rhoad JJ, Raulins NR (1975) Org React 22:1–252
8. Hill RK (1991) Comprehensive organic synthesis. Pergamon, UK
9. Paquette LA (1997) Tetrahedron 53:13971–14020
10. Voegtle F, Goldschmitt E (1976) Chem Ber 109:1–40
11. Carballo RM, Purino M, Ramirez MA, Martin VS, Padron JI (2010) Org Lett 12:5334–5337
12. Overman LE, Kakimoto MJ (1979) J Am Chem Soc 101:1310–1312
13. Zhou L, Li ZM, Zou Y, Wang QR, Sanhueza IA, Schoenebeck F, Goeke A (2012) J Am Chem Soc 134:20009–20012
14. Mu WB, Zhou LJ, Zou Y, Wang QR, Goeke A (2014) Eur J Org Chem 11:2379–2385
15. Delso I, Melicchio A, Isasi A, Tejero T, Merino P (2013) Eur J Org Chem 25:5721–5730
16. Frisch MJ, Trucks GW, Schlegel HB, Scuseria GE, Robb MA, Cheeseman JR, Scalmani G, Barone V, Mennucci B, Petersson GA, Nakatsuji H, Caricato M, Li X, Hratchian HP, Izmaylov AF, Bloino J, Zheng G, Sonnenberg JL, Hada M, Ehara M, Toyota K, Fukuda R, Hasegawa J, Ishida M, Nakajima T, Honda Y, Kitao O, Nakai H, Vreven T, Montgomery JA, Peralta JE, Ogliaro F, Bearpark M, Heyd JJ, Brothers E, Kudin KN, Staroverov VN, Kobayashi R, Normand J, Raghavachari K, Rendell A, Burant JC, Iyengar SS, Tomasi J, Cossi M, Rega N, Millam JM, Klene M, Knox JE, Cross JB, Bakken V, Adamo C, Jaramillo J, Gomperts R, Stratmann RE, Yazyev O, Austin AJ, Cammi R, Pomelli C, Ochterski JW, Martin RL, Morokuma K, Zakrzewski VG, Voth GA, Salvador P, Dannenberg JJ, Dapprich S, Daniels AD, Farkas Ö, Foresman JB, Ortiz JV, Cioslowski J, Fox DJ (2009) Gaussian 09, revision A.02. Gaussian Inc., Wallingford, CT
17. Dunning TH, Hay PJ (1977) Modern theoretical chemistry. Plenum, New York
18. Igel-Mann G, Stoll H, Preuss H (1988) Mol Phys 65:1321–1328
19. Becke AD (1993) J Chem Phys 98:5648–5652
20. Stephens PJ, Devlin FJ, Chabalowski CF, Frisch MJ (1994) J Phys Chem 98:11623–11627
21. Lee C, Yang W, Parr RG (1988) Phys Rev B 37:785–789
22. Gonzalez C, Schlegel HB (1989) J Chem Phys 90:2154–2161
23. Gonzalez C, Schlegel HB (1990) J Phys Chem 94:5523–5527
24. Barone V, Cossi M (1998) J Phys Chem A 102:1995–2001
25. Cances E, Mennunci B, Tomasi J (1997) J Chem Phys 107:3032–3041
26. Cossi M, Barone V, Cammi R, Tomasi J (1996) Chem Phys Lett 255:327–335
27. Barone V, Cossi M, Tomasi J (1998) J Comput Chem 19:404–417
28. Takano Y, Houk KN (2005) J Chem Theory Comput 1:70–77
29. Reed AE, Weinstock RB, Weinhold F (1985) J Chem Phys 83:735–746
30. Glendening ED, Badenhoop JK, Reed AE, Carpenter JE, Bohmann JA, Morales CM, Weinhold F, Morales M, Weinhold F (2010) NBO 5.9. Theoretical Chemistry Institute, University of Wisconsin, Madison
31. Jacobsen H (2008) Can J Chem 86:695–702
32. Johnson ER, Keinan S, Mori-Sanchez P (2010) J Am Chem Soc 132:6498–6506
33. Lu T (2011) Multiwfn Version 2.1. University of Science and Technology Beijing, China, WI
34. Crane EA, Scheidt KA (2010) Angew Chem Int Ed 49:8316–8326
35. Miranda PO, Ramirez MA, Martin VS, Padron JI (2008) Chem Eur J 14:6260–6268
36. Celebi-Olcum N, Ess DH, Aviyente V, Houk KN (2008) J Org Chem 73:7472–7480
37. Li Y, Houk KN (1993) J Am Chem Soc 115:7478–7485
38. Houk KN, Lin YT, Brown FK (1986) J Am Chem Soc 108:554–556
39. Woodward RB, Katz TJ (1959) Tetrahedron 5:70–89
40. Zou Y, Mouhib H, Stahl W, Goeke A, Wang QR, Kraft P (2012) Chem Eur J 18:7010–7016
41. Zhao Y, Truhlar DG (2008) Acc Chem Res 41:157–167
42. Li ZM, Wang QR (2011) Int J Quantum Chem 111:3805–3815

43. Domingo LR, Saez JA (2009) Org Biomol Chem 7:3576–3583
44. Gorelsky SI, Ghosh S, Solomon EI (2006) J Am Chem Soc 128:278–290
45. Ess DN, Houk KN (2007) J Am Chem Soc 129:10646–10647
46. Van-Zeist WJ, Bickelhaupt FM (2010) Org Biomol Chem 8:3118–3127
47. Gorelsky SI, Lapointe D, Fagnou K (2012) J Org Chem 77:658–668